Proceedings of 15th International Marine Design Conference (IMDC-2024)
June 2-6, 2024
Amsterdam, the Netherlands

Hydrodynamics of an Underwater Vehicle Near the Sea Surface

Mavrakos S. Anargyros[1,2], Konispoliatis N. Dimitrios[2*], Rossides George[3], Mavrakos A. Spyridon[2]

ABSTRACT

The primary goal of this study is to evaluate the hydrodynamic characteristics and the wave exciting forces on a shallowly submerged vehicle. A thin, rigid plate, which is completely submerged beneath the free surface in waters of finite depth is considered herein. The examined body is similar to an unmanned vehicle which is developed in Cyprus Marine and Maritime Institute for ocean science applications. From the present analysis the phenomenon of negative added mass and rapid variations of the added mass and damping coefficients is verified due to the free surface effect which is explained in terms of near-resonant standing waves above the submerged body.

KEY WORDS

Hydrodynamics; Exciting Forces; Added Mass; Damping Coefficient; Submerged Structure.

1. INTRODUCTION

Studying the hydrodynamic characteristics of bodies submerged near to the sea surface is especially crucial for specific scenarios in ocean engineering. Specifically, the maneuverability and control of unmanned underwater vessels when they interact with the sea surface become critical for safe operations, requiring accurate prediction of hydrodynamic loading and vessel motion characteristics. However, motion maneuvering analysis is traditionally focused on surface vessels and submerged bodies floating far away from the free surface. On the other hand, little analysis is available on the case where a vessel is floating near the free surface.

As early as 1960s Ogilvie (1963) presented a two-dimensional analysis concerning horizontal cylindrical bodies with circular or square cross sections submerged near the free water surface, concluding to a negative hydrodynamic (added) mass occurrence. In addition, Chung (1977) conducted experiments on a two-dimensional submerged circular or square cross section which was forced to oscillate in sway and heave directions for several submergences below free water surface. He illustrated negative added mass values for a square section when the submergence was on quarter of the semi-width. Newman et al. (1984) explained the occurrence of negative added mass values, along with rapid variations in the damping and added mass coefficients for certain frequency ranges, based on the resonant free surface motion observed in the fluid region above a submerged body. Similar physical argumentation was applied by Mavrakos (1993) in order to explain the negative added mass and sharp peaks of the force coefficients and the hydrodynamic characteristics of groups of interacting axisymmetric submerged bodies near the free surface or the seabed. Recently, a self-regulating fuzzy depth control method was developed by Shao et al. (2012) in order to maintain a cylindrical submerged structure at a specific depth below the free water surface, under free surface disturbances.

Fully submerged objects moving near the free surface deform the water surface and create propagating waves that carry away energy. This dissipation of energy leads to a resisting force known as wave drag force. The problem was theoretically treated by Michell (1898) and Havelock (1917, 1931) for spheres and spheroids, whereas Chepelianskii et al. (2010) addressed the

[1] Inlecom Group, Brussels, Belgium; 0000-0002-8290-9861
[2] Laboratory for Floating Structures and Mooring Systems. Division of Marine Structures, School of Naval Architecture and Marine Engineering, National Technical University of Athens, Athens, Greece; 0000-0001-7256-513X; 0000-0002-7250-9581
[3] Cyprus Marine and Maritime Institute, Larnaca, Cyprus; 0000-0003-0522-812X
* Corresponding Author: *dkonisp@naval.ntua.gr*

Submitted: 16 February 2024, Revised: 17 April 2024, Accepted: 1 May 2024, Published: 21 May 2024

Conference paper, DOI: https://doi.org/10.59490/imdc.2024.861 e-ISSN: 3050-4864

influence of an immersed cylinder on wave propagation based on the analysis on submerged spheres. Also, Benusiglio et al. (2015) used fully submerged spheres to study the effect of the wave drag near the free surface. It was emphasized that the wave drag was comparable in magnitude to the hydrodynamic drag when the top of the sphere was at less than one sphere radius from the surface.

Although little analysis is available on submerged axisymmetric cylindrical/spherical bodies near the free surface, the movement of submarines in a near-surface water environment has been the subject of many studies in the literature. Submarines descend to periscope or snorkeling depth for target exploration or battery recharging. In such scenarios environmental loads like waves, currents, resistance and suction forces are imposed on the submerged structure (Arentzen and Mandel, 1960; Burcher and Rydill, 1995). Several studies have been presented in the literature investigating the impact of the free water surface on an underwater vehicle through both numerical and experimental methods. Indicatives are Jagadeesh et al., 2009; Manssorzadeh and Javanmard, 2014; Nematollahi et al., 2015; Conway et al. 2018; Amiri et al., 2018, 2019a, 2019b, 2020; Lambert et al. 2020; Sudharsun et al. 2022; Ling et al. 2023. Furthermore, since the imposed forces on a submerged structure are different from those in large water depths, submarines are required to keep the necessary navigating pose (depth, roll angle and trim angle). Consequently, numerous research activities on depth control have been performed. Specifically, Hao et al. (2004) developed a two-step depth fuzzy controller to produce stern angle to counteract the second-order exciting wave forces on a submarine, whereas Choi et al. (2006, 2008) proposed a mathematical model for the evaluation of the wave exciting forces on a submerged structure and performed depth control simulations using the proportional-integral-derivative method. Rezazadegan et al. (2015) proposed a novel adaptive trajectory tracking control of an autonomous underwater vehicle in six-degree of freedom. In addition, Park et al. (2016) elaborated an adaptive control technique utilizing a neural network and a proportional-integral-derivative controller to regulate the depth of a submerged body in close proximity to free water surface. At the same time, the case of the water surface being covered with ice has also been considered. Zemlyak et al. (2021, 2023) studied theoretically and experimentally the motions of a submerged body near the free water surface when the latter was covered by ice. Here a sink-source model was applied, and the ice cover was simulated as a thin elastic plate floating on the water surface, whereas the experiments were performed in an ice tank. It was concluded that the variation of the relative submergence of a body moving at a shallow submergence attained non negligible values.

The main objective of this investigation is to evaluate the hydrodynamic characteristics and the wave exciting forces on a shallowly submerged vehicle. A thin, rigid plate, which is completely submerged beneath the free surface in waters of finite depth is considered herein. The examined body is similar to an unmanned vehicle which is developed in Cyprus Marine and Maritime Institute (CMMI) for ocean science applications. In the present analysis a semi-theoretical formulation is described by properly composing the solutions of the diffraction and the motion radiation problems around the floating structure within the framework of linear potential theory. This is done under the assumption of an incompressible and inviscid fluid and an irrotational flow. In addition, two numerical simulation tools, ANSYS Aqwa and HAQi software, are also implemented to compare the numerical results with the theoretical ones.

The rest of this paper is structured as follows. In Section 2 the geometric model of the underwater vehicle is introduced. Section 3 presents the developed theoretical formulation within the domain of linear potential theory, whereas focus is also given to the applied numerical models. Section 4 is dedicated to the presentation of the outcomes of the two applied formulations whereas conclusions of the work are drawn in Section 5.

2. DESCRIPTION OF THE CONSIDERED AUTONOMOUS UNDERWATER VEHICLE

Underwater gliders are autonomous vehicles that move through the water by changing their buoyancy and pitch (Javaid et al., 2014), which makes them more energy-efficient than other types of autonomous marine vehicles (AMVs) while minimizing their acoustic signature. This makes them ideal for many oceanic surveying applications, including long-term environmental monitoring, marine animal tracking and oceanographic surveying (Javaid et al., 2014). Additionally, gliders are relatively low-cost and can be deployed for extended periods.

The traditional torpedo-shaped underwater gliders are limited by their slow speed and restricted maneuverability, which can make them unsuitable for some applications (Javaid et al., 2014). To address some of these limitations, Disk-Type Underwater Gliders (DTUG) emerged (Nakamura et al., 2007, 2008; Yu et al., 2017; Zhou et al., 2020). Unlike torpedo-shaped gliders, DTUGs have omnidirectional motion capabilities, which make them more maneuverable and better suited for navigating complex underwater environments, such as near islands or inside narrow channels. An important example of such a marine environment is the Aegean Sea, where the existence and close proximity of large and small islands and rocky islets as well as the dense marine traffic (both for commercial and leisure purposes), require autonomous vehicles that operate in this region to have high-manoeuvrability capabilities. The Cyprus Marine and Maritime Institute is exploring the DTUG trend through the design and implementation of its own DTUG prototype, which has diameter of 5.2m and overall height of 0.86m, as shown in Figure 1, specifically for use in the Aegean Sea and eastern Mediterranean regions.

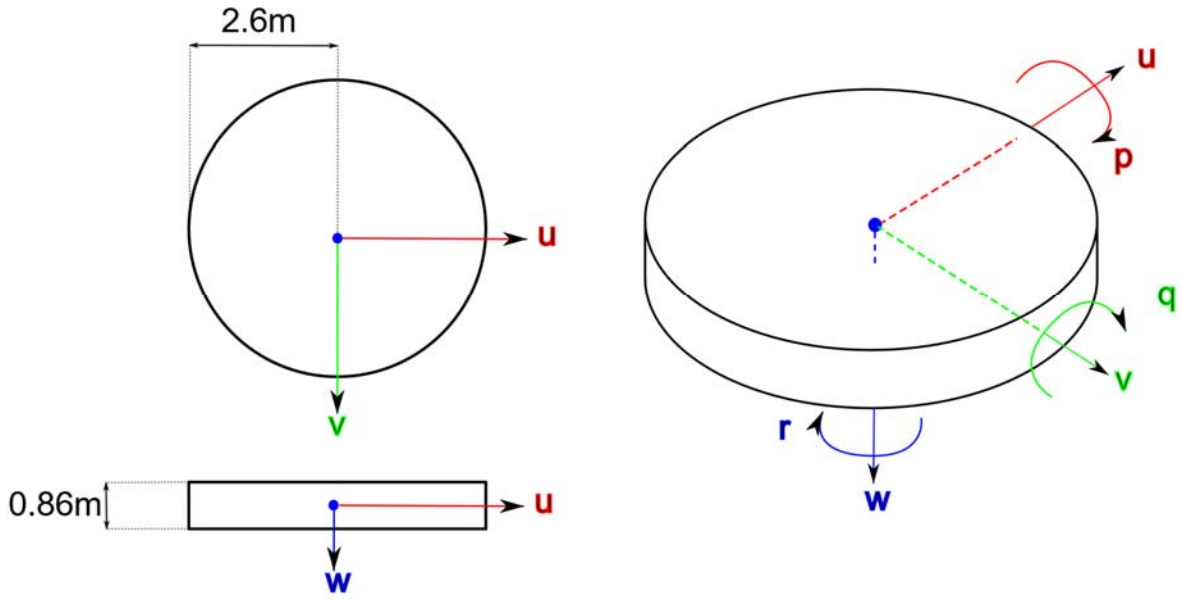

Figure 1: Schematic representation of the examined Disk-Type Underwater Glider

The large size of the DTUG enables it to carry high-volume buoyancy engines, which in turn allow it to navigate while carrying large payloads of more than 200kg, including components of energy harvesting technologies that can enhance its overall power autonomy. Additionally, its flat and wide structure offers stealth capabilities when the DTUG lies on the ocean surface, since it can become nearly invisible to both underwater and above surface detection methods (e.g., underwater sonar and above-surface radar).

The existence of negative hydrodynamic (added) mass and excitation forces that can occur near the ocean surface can enable the DTUG to maintain its shallow depth without the need for additional consumption of energy. At the same time, to achieve full submersion away from the ocean surface, these hydrodynamic effects need to be overcome. The creation of a comprehensive autonomous controller that can properly utilize or overcome these hydrodynamic effects depending on the mission needs of the DTUG, requires the proper understanding of the magnitude and occurrence of these effects under different situations.

According to Fossen (2011), from a maneuvering theory perspective, the 6 DOF motion model of an underwater vehicle is given by:

$$\boldsymbol{M\dot{v} + C(v)v + D(v)v + g(x) = \tau + \tau_{wave}}, \quad (1)$$

where $\boldsymbol{v} = [u, v, w, p, q, r]$ is the glider's velocity vector in the body frame, as shown in Figure 1, while $\boldsymbol{x} = [x, y, z, \varphi, \theta, \psi]$ is the glider's position and orientation vector in the inertial frame. $\boldsymbol{M = M_{RB} + M_A} \in \mathbb{R}^{6x6}$ is the system inertia matrix, $\boldsymbol{C(v)} \in \mathbb{R}^{6x6}$ is a skew-symmetric matrix describing the Coriolis and centripetal effects due to the motion of the glider and $\boldsymbol{D(v) = D_P + D_V + D_n(v)} \in \mathbb{R}^{6x6}$ is a positive-semidefinite symmetric matrix denoting the (potential, linear and quadratic) damping forces. It should be noted that quadratic damping forces (described by the $\boldsymbol{D_n(v)}$ matrix) are largely excluded from the motion model of underwater gliders, due to the very low maximum speeds that they can reach. Additionally, forces occurring by Coriolis and centripetal effects (described by the $\boldsymbol{C(v)}$ matrix) can be also assumed to be negligible due to the low maximum speeds of the vehicle. These simplification assumptions are further strengthened in the case of DTUGs, where their omnidirectional motion characteristics allow for small deviations between the actual motion of the DTUG and its modelled behaviour, caused by such forces, to be easily corrected as soon as they occur.

The vector $\boldsymbol{g(x)} \in \mathbb{R}^6$ describes the gravitational/buoyancy forces and moments acting on the underwater vehicle, while the vector $\boldsymbol{\tau} \in \mathbb{R}^6$ describes its actuation forces and moments. In the case of underwater gliders, the actuation of the vehicle occurs through the manipulation of its gravitational/buoyancy forces and moments and thus the two terms can be merged. Lastly, the vector $\boldsymbol{\tau_{wave}} \in \mathbb{R}^6$ describes the excitation forces acting on the glider when it operates at water depths close to the ocean surface, inside the wave-affected zone. Therefore, the simplified motion model of the DTUG takes the form:

$$\boldsymbol{[M_{RB} + M_A]\dot{v} + [D_P + D_V]v + g(x) = \tau_{wave}} \quad (2)$$

$\boldsymbol{M_{RB}}$ represents the rigid body mass and inertia and assuming that the centre of gravity (CG) of the vehicle is at the origin of its body frame, it is given by:

$$\boldsymbol{M_{RB}} = \begin{bmatrix} m & 0 & 0 & & & \\ 0 & m & 0 & & 0 & \\ 0 & 0 & m & & & \\ & & & I_x & -I_{xy} & -I_{xz} \\ & 0 & & -I_{yx} & I_y & -I_{yz} \\ & & & -I_{zx} & -I_{zy} & I_z \end{bmatrix} \tag{3}$$

$\boldsymbol{M_A}$ is the hydrodynamic (added) mass matrix which can be approximated using the potential coefficients $\boldsymbol{A}(\omega)$ by:

$$\boldsymbol{M_A} \approx \begin{bmatrix} A_{11}(0) & 0 & & \cdots & & 0 \\ 0 & A_{22}(0) & & & & A_{26}(0) \\ & & A_{33}(\omega_{heave}) & 0 & 0 & \\ & \vdots & 0 & A_{44}(\omega_{roll}) & 0 & \vdots \\ & & 0 & 0 & A_{55}(\omega_{pitch}) & \\ 0 & A_{62}(0) & & \cdots & & A_{66}(0) \end{bmatrix} \tag{4}$$

where the natural frequencies ω_{heave}, ω_{roll} and ω_{pitch} depend on the hydrostatic characteristics of the vehicle in the centre of flotation (CF) (Fossen, 2011). Due to the actuation characteristics of underwater gliders, their CF may be continuously varying throughout their operation. Describing the internal configuration of the actuation elements of the studied DTUG is beyond the scope of this paper and therefore, further analysis on how the aforementioned natural frequencies can be obtained will not be presented.

Like $\boldsymbol{M_A}$, the potential damping matrix $\boldsymbol{D_P}$ can be approximated using the potential coefficients $\boldsymbol{B}(\omega)$ by:

$$\boldsymbol{D_P} \approx \begin{bmatrix} 0 & 0 & & \cdots & & 0 \\ 0 & 0 & & & & 0 \\ & & B_{33}(\omega_{heave}) & 0 & 0 & \\ \vdots & & 0 & B_{44}(\omega_{roll}) & 0 & \vdots \\ & & 0 & 0 & B_{55}(\omega_{pitch}) & \\ 0 & 0 & & \cdots & & 0 \end{bmatrix} \tag{5}$$

On the other hand, the linear viscous damping matrix $\boldsymbol{D_V}$ is usually approximated by a diagonal matrix:

$$\boldsymbol{D_V} \approx \text{diag}\{B_{11v}, B_{22v}, B_{33v}, B_{44v}, B_{55v}, B_{66v}\} \tag{6}$$

where the elements B_{iiv} $(i = 1, \dots 6)$ depend on the potential coefficients $\boldsymbol{A}(\omega)$ and can be computed from the time constants and natural periods of the vehicle (Fossen, 2011). Once again, further elaboration on the methods used to obtain the time constants and natural periods of the vehicle, requires a description of its internal actuation elements, which lies beyond the scope of this paper.

The presented manoeuvering theory applies to vehicles operating at water depths below the wave-affected zone and it results in reduced model complexity to enable real-time motion prediction and control. To achieve this reduced complexity, the theory assumes no coupling between the surge, heave-roll-pitch and the sway-yaw subsystems, which in turn excludes the use of the potential coefficients $A_{15}, A_{51}, A_{24}, A_{42}, B_{15}, B_{51}, B_{24}$ and B_{42} from Equations (4) and (5).

Conversely, motion control near the sea surface is limited due to the way of actuation of DTUGs and it primarily involves motion along their heave-roll-pitch degrees of freedom (i.e., using the potential coefficients $A_{33}, A_{44}, A_{55}, B_{33}, B_{44}, B_{55}$) while also considering possible wave-excitation forces. That said, the calculation of other significant potential coefficients ($A_{15}, A_{51}, A_{24}, A_{42}, B_{15}, B_{51}, B_{24}$ and B_{42}) can enable further DTUG functionalities to be developed in the future. More specifically, using advanced parameter-estimation algorithms along with a more detailed motion model, it is expected that the vehicle will be able to accurately estimate the current sea-state, based on its past motion, both for oceanographic surveying applications and in order to be able to submerge itself in unfavourable weather conditions. To this end, the rest of this paper will focus on the study of all significant potential coefficients $\boldsymbol{A}(\omega)$ and $\boldsymbol{B}(\omega)$ for the studied DTUG.

3. FORMULATION OF THE PROBLEM

3.1 Theoretical Formulation

We consider a cylindrical submerged disk with vertical axis of symmetry, similar to the above DTUG, which is exposed to the action of regular waves propagating in water depth d with frequency ω. A cylindrical co-ordinate system (r, θ, z) is defined with origin on the sea bottom and its vertical axis Oz directed upwards (Figure 2). Let the linear translation and rotational

vector of the body's motion be denoted by $\boldsymbol{\xi} = (\xi_1, \xi_2, \xi_3)$ and $\boldsymbol{\theta} = (\xi_4, \xi_5, \xi_6)$, respectively. Their components correspond to the surge (j = 1), sway (j =2), heave (j =3), roll (j = 4), pitch (j = 5) and yaw (j =6) modes of motion. Under the assumption of a symmetrical mass distribution, a vertical cylindrical body undergoes three-degree of freedom motion in the wave propagation plane under the influence of a regular wave train, i.e. two translations (surge, ξ_1; heave, ξ_3) and one rotation (pitch, ξ_5).

Assuming further that the viscous effects are negligible, the fluid is incompressible, and the displacements of the body and the wave height are small, classical linearized water wave theory can be employed. The fluid flow can be delineated by the potential function:

$$\Phi(r, \theta, z; t) = Re[\varphi(r, \theta, z).\, e^{-i\omega t}] \tag{7}$$

where the complex potential function $\varphi(r, \theta, z)$ can be expressed, on the basis of linear modelling, as a superposition of the incident, φ_0, scattered, φ_7, and radiated wave fields due to the motion of the body, i.e.

$$\varphi = \varphi_0 + \varphi_7 + \sum_{j=1,3,5} \dot{\xi}_{j0}\, \varphi_j = \varphi_D + \sum_{j=1,3,5} \dot{\xi}_{j0}\, \varphi_j \tag{8}$$

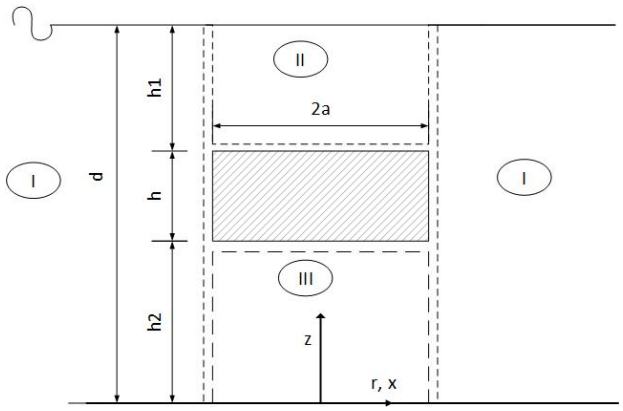

Figure 2: Submerged disk. Definitions and discretization of the flow field around the body.

Here, φ_j denotes the potential of the wave field due to the forced oscillation of the body in the *j* th mode of motion with unit velocity amplitude $\dot{\xi}_{j0}$. Moreover, all contributions to the total potential φ must be solutions of the Laplace's equation in the entire fluid domain and must meet the following boundary conditions:

$$\omega^2 \varphi_D - g\, \frac{\partial \varphi_D}{\partial z} = \omega^2 \varphi_j - g\, \frac{\partial \varphi_j}{\partial z} = 0, \quad z = d, \quad j = 1, 3, 5 \tag{9}$$

$$\frac{\partial \varphi_D}{\partial z} = \frac{\partial \varphi_j}{\partial z} = 0, \quad z = 0, \quad j = 1, 3, 5 \tag{10}$$

$$\frac{\partial \varphi_D}{\partial \boldsymbol{n}} = 0, \quad on\ S \tag{11}$$

$$\frac{\partial \varphi_j}{\partial \boldsymbol{n}} = n_j, \quad on\ S, \quad j = 1, 3, 5 \tag{12}$$

Where $\partial(\ )/\partial \boldsymbol{n}$ stands for the derivative in the direction of the outward unit normal vector $\boldsymbol{n}$ to the mean wetted surface *S* of the body and n_j are its generalized normal components specified by:

$$\boldsymbol{n} = (n_1, n_2, n_3), \quad \boldsymbol{r}\, \boldsymbol{x}\, \boldsymbol{n} = (n_4, n_5, n_6) \tag{13}$$

$\boldsymbol{r}$ is the position vector of a point on *S* with respect to the body's reference point of motion expressed in the co-ordinate system (*r, θ, z*). Finally, a radiation condition must be enforced stipulating that propagating disturbances must be outgoing.

The velocity potential of the undisturbed incident wave system, φ_0 propagating along the positive x – axis can be described in the cylindrical co-ordinate system (*r, θ, z*) as follows:

$$\varphi_0(r,\theta,z) = -i\omega A \frac{Z_0(z)}{Z_0'(d)} \sum_{m=0}^{\infty} \varepsilon_m i^m J_m(kr)\cos(m\theta) \tag{14}$$

In Equation (14), A denotes the wave amplitude, ε_m is the Neumann's symbol (i.e., $\varepsilon_0 = 1;\ \varepsilon_m = 2$ for $m > 0$), J_m is the mth order Bessel function of first kind, Z_0 equals to:

$$Z_0(z) = N_0^{-1/2}\cosh(kz) = \left[\frac{1}{2}\left[1 + \frac{\sinh(2kd)}{2kd}\right]\right]^{-\frac{1}{2}}\cosh(kz) \tag{15}$$

and $Z_0'(d)$ denotes Z_0 derivative at $z = d$. The wave number k is associated with the wave frequency ω by the dispersion equation: $\omega^2 = kg\tanh(kd)$.

For solving the diffraction and radiation problems, the method of matched axisymmetric eigenfunction expansions will be utilized. As per the method, the flow around the submerged cylinder is subdivided into cylinder - shaped fluid regions, denoted by I, II, III (see Figure 2), where appropriate series representations of the fluid's velocity potential in cylindrical co-ordinates will be established.

In accordance with the series representation of the undisturbed incident wave potential, eq. (14), the diffraction potential at each fluid region $\ell = I, II, III$ is anticipated to:

$$\varphi_D^l(r,\theta,z) = -i\omega A \sum_{m=0}^{\infty} \varepsilon_m i^m \Psi_{Dm}^{\ell}(r,z)\cos(m\theta) \tag{16}$$

while for the radiation velocity potential φ_j^p at each fluid domain, ℓ, yields:

$$\varphi_j^l(r,\theta,z) = \sum_{m=0}^{\infty} \Psi_{jm}^{\ell}(r,z)\cos(m\theta)\,,\ j = 1,3,5 \tag{17}$$

In the unknown functions Ψ_{jm}^{ℓ} (see Equations (16) and (17)), the first subscript $j = D, 1, 3, 5$ signifies the representative boundary value problem being considered, while the second subscript the m values that need to be taken into account. It is worth noting that the fluid flow resulting from the forced oscillation of the cylinder in still water, is symmetric about $\theta = 0$ - plane and antisymmetric about $\theta = \frac{\pi}{2}$ -plane for surge (j = 1) and pitch (j = 5) mode of motions, whereas it is symmetric with respect to both these planes for heave mode, (j = 3). Hence, Equation (17) can be rewritten as:

$$\varphi_j^l(r,\theta,z) = \Psi_{j1}^{\ell}(r,z)\cos(\theta),\ j = 1{,}5 \tag{18}$$

$$\varphi_3^l(r,\theta,z) = \Psi_{30}^{\ell}(r,z),\ j = 3 \tag{19}$$

To evaluate the unknown functions Ψ_{jm}^{ℓ} the method of separation of variables for the Laplace differential equation is employed. Consequently, suitable series representations of the functions $\Psi_{jm}^{\ell}, j = D, 1, 3, 5;\ \ell = I, II, III$ in each fluid domain around the submerged disk can be established (Kokkinowrachos, et al, 1986; Mavrakos, 1985, 1988, 2004)

(a) Outer fluid domain I $(r \geq a, 0 \leq z \leq d)$

$$\frac{1}{\delta_j}\Psi_{jm}^{I}(r,z) = g_{jm}^{I}(r,z) + \sum_{n=0}^{\infty} F_{jmn}^{I} \frac{K_m(a_n r)}{K_m(a_n a)} Z_n(z) \qquad \text{for } j=D,\ 1,\ 3,\ 5; \tag{20}$$

where:

$$g_{Dm}^{I}(r,z) = \left\{J_m(kr) - \frac{J_m(ka)}{H_m(ka)}H_m(kr)\right\}\frac{Z_0(z)}{d\dot{Z}_0(d)}\ ; \qquad g_{11}^{I}(r,z) = g_{30}^{I}(r,z) = g_{51}^{I}(r,z) = 0 \tag{21}$$

and $\delta_D = \delta_1 = \delta_2 = \delta_3 = d,\ \delta_4 = \delta_5 = d^2$; H_m, K_m are the m-th order Hankel function of first kind and the modified Bessel function of second kind, respectively. Also, F_{jmn}^{I} are the unknown Fourier coefficients to be established by the solution process. Moreover,

$$Z_n(z) = \left[\frac{1}{2}\left[1 + \frac{\sin(2a_n d)}{2a_n d}\right]\right]^{-1/2} \cos(a_n z), n \geq 1 \tag{22}$$

The eigenvalues a_n are roots of the transcendental equation: $\omega^2 + g a_n \tan(a_n d) = 0$, which possesses one imaginary, $a_0 = -ik, k > 0$ and infinite number of real roots.

(b) For the fluid domain of type *II* ($0 \leq r \leq a, h_2 + h \leq z \leq d$

$$\frac{1}{\delta_j}\Psi_{jm}^{II}(r,z) = g_{jm}^{II}(r,z) + \sum_{q=0}^{\infty} F_{jmq}^{II} \frac{I_m(a_q r)}{I_m(a_q a)} Z_q(z) \qquad \text{for } j = \text{D, 1, 3, 5} \tag{23}$$

where:

$$g_{Dm}^{II}(r,z) = g_{11}^{II}(r,z) = 0; \quad g_{30}^{II}(r,z) = \frac{z}{d} - 1 + \frac{g}{d\omega^2}; \quad g_{51}^{III}(r,z) = -\frac{r}{d^2}\left[(z-d) + \frac{g}{\omega^2}\right] \tag{24}$$

and $\delta_D = \delta_1 = \delta_2 = \delta_3 = d$, $\delta_4 = \delta_5 = d^2$; I_m , the *m*-th order modified Bessel function of first kind. Here F_{jmq}^{II} denote the unknown Fourier coefficients to be determined by the solution process. Additionally,

$$Z_q(z) = \left[\frac{1}{2}\left[1 + \frac{\sin(2a_q(d-(h+h_2)))}{2a_q(d-(h+h_2))}\right]\right]^{-1/2} \cos\left[a_q\left(z - (h + h_2)\right)\right], q \geq 1 \tag{25}$$

The eigenvalues a_q are roots of the transcendental equation: $\omega^2 + g a_q \tan\left[a_q\left(z - (h + h_2)\right)\right] = 0$, which possesses one imaginary, $a_0 = -ik_{II}$, $k_{II} > 0$ and infinite number of real roots.

(c) For the fluid domain of type *III*

$$\frac{1}{\delta_j}\Psi_{jm}^{III}(r,z) = g_{jm}^{III}(r,z) + \sum_{p=0}^{\infty} \varepsilon_p F_{jmp}^{III} \frac{I_m\left(\frac{p\pi r}{h_2}\right)}{I_m\left(\frac{p\pi a}{h_2}\right)} cos\left(\frac{p\pi z}{h_2}\right) \tag{26}$$

where:

$$g_{Dm}^{III}(r,z) = g_{11}^{III}(r,z) = 0; \; g_{30}^{III}(r,z) = \frac{z^2 - (\frac{1}{2})r^2}{2h_2 d}; \; g_{51}^{III}(r,z) = -\frac{r\left[z^2 - (\frac{1}{4})r^2\right]}{2h_2 d^2} \tag{27}$$

δ_j, $j = D, 1, 3, 5$, is defined above and ε_p is the Newmann's symbol, see eq. (8); F_{jmp}^{III} are the unknown Fourier coefficients to be determined through the solution process. In Equations (20), (23) and (26), $g_{jm}^{l}(r,z)$, l = *I, II, III* and j =1, 3, 5 represent particular solutions for the different mode of motions, which satisfy the respective kinematic conditions on the horizontal boundaries of the fluid domains of types *I, II* and *III.* The same is valid for the homogeneous parts of the series expansions of the velocity potential representations, see Equations (20), (23) and (26), which are properly selected so that the kinematic boundary conditions on the horizontal walls of the cylindrical body, the linearized dynamic condition on the free surface, see Equation (9), and the kinematic one on the seabed, see Equation (10), are satisfied beforehand. Employing Galerkin's method the potential solutions are aligned by ensuring continuity of hydrodynamic pressure and radial velocity at the vertical boundaries of adjacent fluid regions. Additionally, kinematic conditions on the bodies' wetted surfaces are satisfied. The methodology has been thoroughly detailed in prior publications for both the diffraction and the radiation problems (Kokkinowrachos, et al, 1986; Mavrakos, 1985, 1988, 2004) and thus, it will be no further elaborated in the present study.

Considering the extreme positions of the cylindrical disk near the free surface, i.e. $h_1 \to 0$, special attention has to be paid as the respective arguments of the Bessel functions involved in the series representation (23) become too large. To circumvent the difficulty, asymptotic expressions for the Bessel functions for large arguments are introduced (Abramowitz and Stegun, 1970) and the corresponding expression for the velocity potential representation in the second fluid domain, i.e. j = *II*, is recast as follows:

$$\frac{1}{\delta_j}\Psi_{jm}^{II}(r,z) = g_{jm}^{II}(r,z) + \sum_{q=0}^{\infty} F_{jmq}^{II} \sqrt{\frac{a}{r}} \frac{e^{a_q r}}{e^{a_q a}} \frac{f_1(a_q r)}{f_1(a_q a)} Z_q(z) \qquad \text{for } j = \text{D, 1, 3, 5} \tag{28}$$

with

$$f_1(z) = 1 - \frac{\mu-1}{8z} + \frac{(\mu-1)(\mu-9)}{2!(8z)^2} - \frac{(\mu-1)(\mu-9)(\mu-25)}{3!(8z)^3} + \cdots. \quad (29)$$

where $\mu = 4m^2$; the rest of the symbols and functions involved in Equation (28) have been defined previously.

3.2 Numerical Formulation

Concerning the numerical formulations, two simulation tools, ANSYS Aqwa and HAQi software, are implemented. ANSYS AQWA is part of ANSYS Mechanical Enterprise suite which performs diffraction and radiation analysis based on potential theory (ANSYS AQWA theory manual, 2015). The physics of AQWA are applicable for finite depth waters and are solved under the frequency domain framework. The version that is used in the present work is the 2021R1. The central processing unit (CPU) time required to achieve the numerical simulation using 17208 wetted elements is about a quarter of a minute for each wave frequency. Figure 3 depicts the element discretization of the examined submerged body.

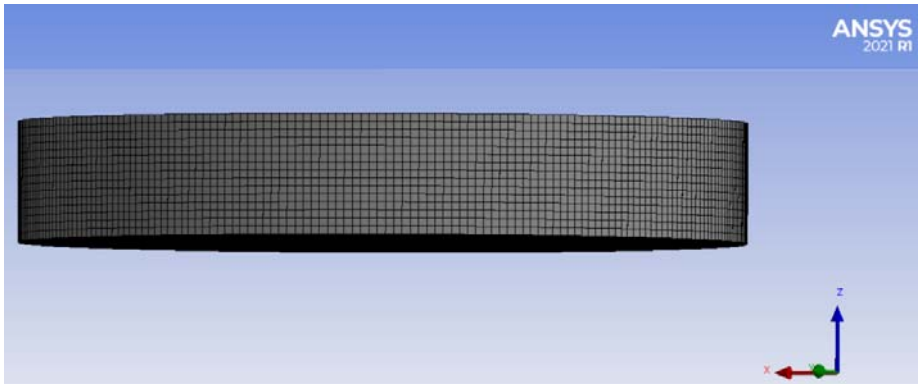

Figure 3: Mesh overview of the examined submerged body for ANSYS AQWA.

HAQi is an in-house developed numerical panel code (Bardis and Mavrakos, 1988) using the sink source technique. Specifically, the velocity potential at every point in the field is derived as the superposition of potentials arising from pulsating singularities (sources) distributed across the wetted surface of the body. Consequently, the fluid potential $\Phi_j, j = 1, \ldots, 6, 7$, around the submerged structure, can be expressed as:

$$\Phi_j(x,y,z) = \frac{1}{4\pi} \iint_{S_0} Q_j(\xi,\eta,\zeta)\, G(x,y,z,\xi,\eta,\zeta) dS\ , j = 1,2,\ldots,6,7 \quad (30)$$

Here $Q_j(\xi,\eta,\zeta)$ is the strength (i.e. density) of the singularity at (ξ,η,ζ); the $G(x,y,z,\xi,\eta,\zeta)$ is the Green function for finite water depth as given in Wehausen and Laitone (1960); $x, y, z, \xi, \eta, \zeta$ are rectangular coordinates, and S_0 is the submerged body's mean wetted surface.

The Laplace differential and the proper boundary conditions are automatically satisfied (see Section 3.1). Hence, the following integral equation can be derived for the diffraction ($j = 7$) and the radiation problems ($j = 1,2, \ldots, 6$), respectively:

$$\frac{1}{2} Q_j(x,y,z) + \frac{1}{4\pi} \iint_{S_0} Q_j(\xi,\eta,\zeta) \frac{\partial G(x,y,z,\xi,\eta,\zeta)}{\partial n} dS = \begin{cases} -\frac{\partial \varphi_0}{\partial n} \text{ for j} = 7 \\ n_i \text{ for j} = 1,2,\ldots,6 \end{cases} \quad (31)$$

Here n_i denote the generalized normal components.

Equation (31) is addressed by subdividing S_0 into plane quadrilateral or triangular elements with singularities positioned at the geometrical center of each element. The integral in Equation (31) is approximated by a finite series of P terms, where P represents the number of plane elements. Consequently, a linear system of P equations is formulated, which is then solved with respect to the source's strengths $Q_j(\xi,\eta,\zeta), j = 1,2,\ldots.,6$. Once $Q_j(\xi,\eta,\zeta)$ has been computed for each element the flow potential can be readily determined from Equation (30). The theoretical framework of this three-dimensional method is extensively described in Wehausen and Laitone (1960); Garrison (1974, 1975); Mavrakos and Bardis (1984), thus it is no further elaborated herein.

The computational workload of the sink-sources formulation can be decreased for bodies with a symmetry plane. Specifically, in the examined case one half of the immerged surface is subdivided. Hence, a total of 266 elements have been considered for the discretization of the half body's wetted surface as can be seen in Figure 4, whereas the CPU time required is about less than a min for each wave frequency.

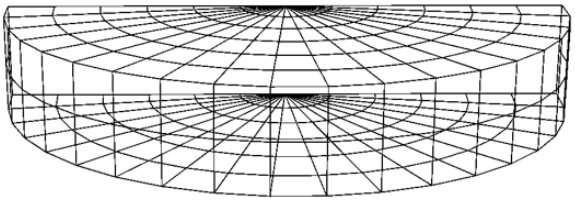

Figure 4: Panel discretization of the examined submerged body for HAQi.

4. NUMERICAL RESULTS

This section compares and discusses the outcomes of the three presented formulations on the hydrodynamics of the submerged unmanned vehicle. The precision of the theoretical modelling is influenced by the evaluation procedure of the Fourier coefficients within each fluid domain surrounding the body. In the present calculations 80 terms are utilized for the series expansions of the velocity potential in the outer I, and upper II, fluid domain, whereas 150 terms are retained for the velocity representation in the lower type III. The theoretical results are acquired using an in-house computer software (Mavrakos, 1995) in FORTRAN programming language. The CPU time is set to less than a second for each analyzed wave frequency.

The geometric characteristics of the considered submerged body are: height of the body h, radius of the body $a = 3.023h$, whereas the water depth $d = 290.7h$. These dimensions have been properly selected based on the geometry of the underwater vehicle developed by the CMMI (see Section 2). Initially, the body is assumed to be floating at $0.116h$ below the free water surface. In Figure 5 the Response Amplitude Operator (RAO) of the exciting wave forces and moments on the submerged vehicle are presented. The depicted results are evaluated by the theoretical formulation and the numerical software.

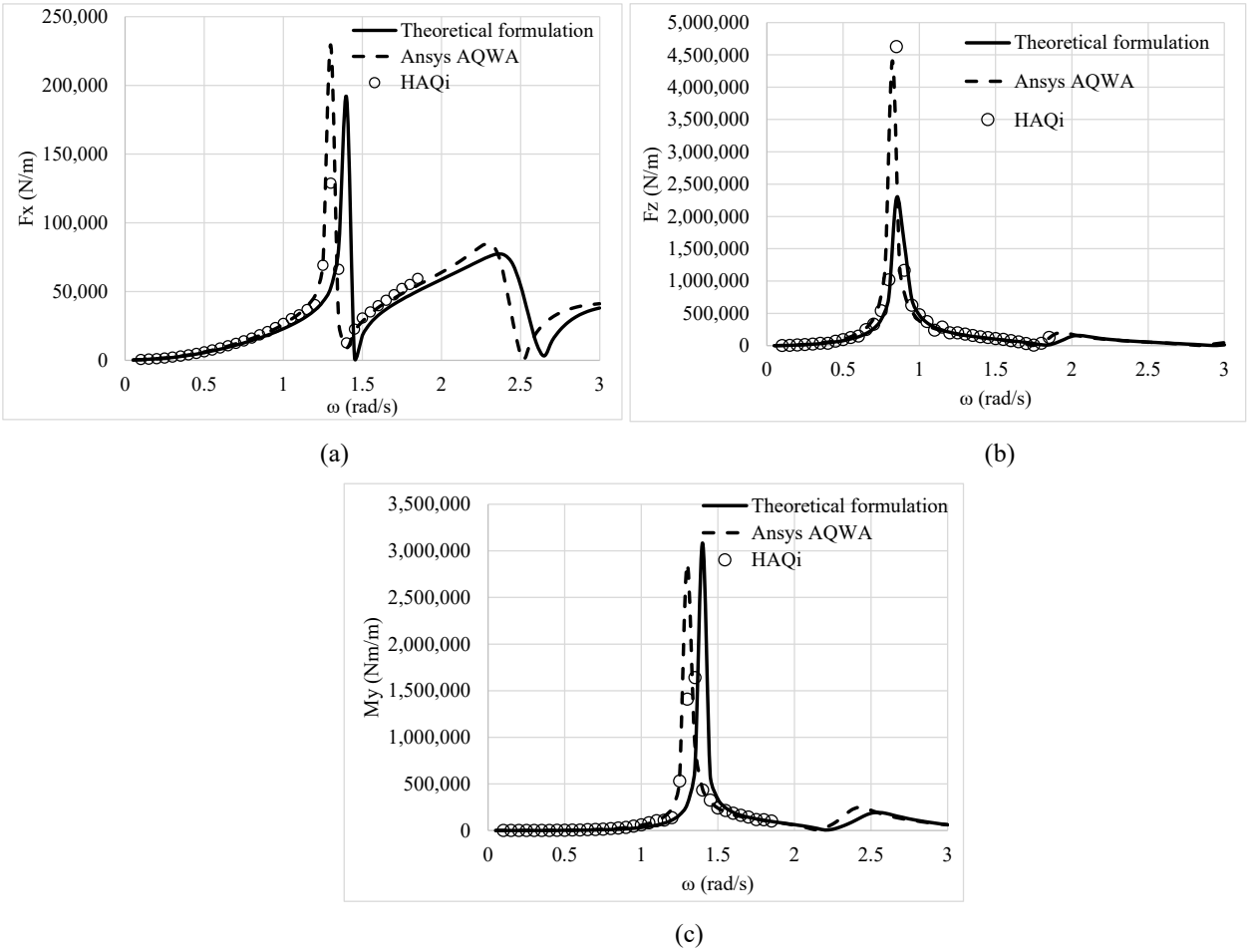

Figure 5: RAO of the exciting forces and moments on the submerged body: (a) horizontal forces; (b) vertical forces; (c) horizontal moments

It is evident from Figure 5a that the horizontal exciting forces show an oscillatory behavior. Specifically in the vicinity of $\omega = 1.3$rad/s the forces depict a quite rapid increase, while a rapid decrease follows leading to a local minimum at $\omega = 1.4$rad/s. The values of F_x exhibit a similar pattern of variation also in the vicinity of $\omega = 2.3$ rad/s and $\omega = 2.4$ rad/s, with a smoother, however, increase and decrease, respectively. It can be also seen from Figure 5c that similar to the surge exciting forces, the sharp peaks observed in horizontal moments are presented at the same wave frequencies. Regarding, the heave exciting forces (see Figure 5b) a smooth variation pattern is depicted with a peak at the neighborhood of $\omega = 0.85$rad/s. As far as the comparisons of the applied methodologies are concerned it can be seen that the results from the numerical software HAQi correlate excellently to the outcomes of AQWA. It is worth noting that certain differences between the results of the theoretical and numerical methods, particularly at wave numbers where the exciting forces reach peaks, can be deemed negligible. This is because the theoretical results are perfectly aligned with the variation pattern observed in the outcomes derived from the numerical formulation.

Figure 6 illustrates the comparison of the added mass coefficients, $A_{11}, A_{33}, A_{55}, A_{15}$ between the theoretical and the numerical models. A strong frequency dependance on the hydrodynamic mass is depicted. The latter is accompanied by sharp peaks at certain frequency ranges. It should be noted that the variation of A_{11} is marked by the occurrence of distinct peaks at the same wave frequencies in which F_x attains maximum and minimum values (see Figure 6a). The same applies to the concerned wave frequency range, where resonance phenomena occur in A_{33} (see Figure 6b). Specifically, A_{33} shows an oscillatory variation pattern at the neighborhood of $\omega = 0.85$rad/s, where the heave exciting forces also attain a peak. Additionally, it is important to note that negative values of the added mass coefficients A_{11}, A_{33}, are depicted near the resonant frequencies. Ogilvie (1963) also observed a similar phenomenon. Regarding the comparisons between the applied methodologies, it can be obtained that the two numerical approaches attain similar results. However, discrepancies between the results of the numerical and the theoretical methods are notable, especially at the vicinity of the resonant frequencies.

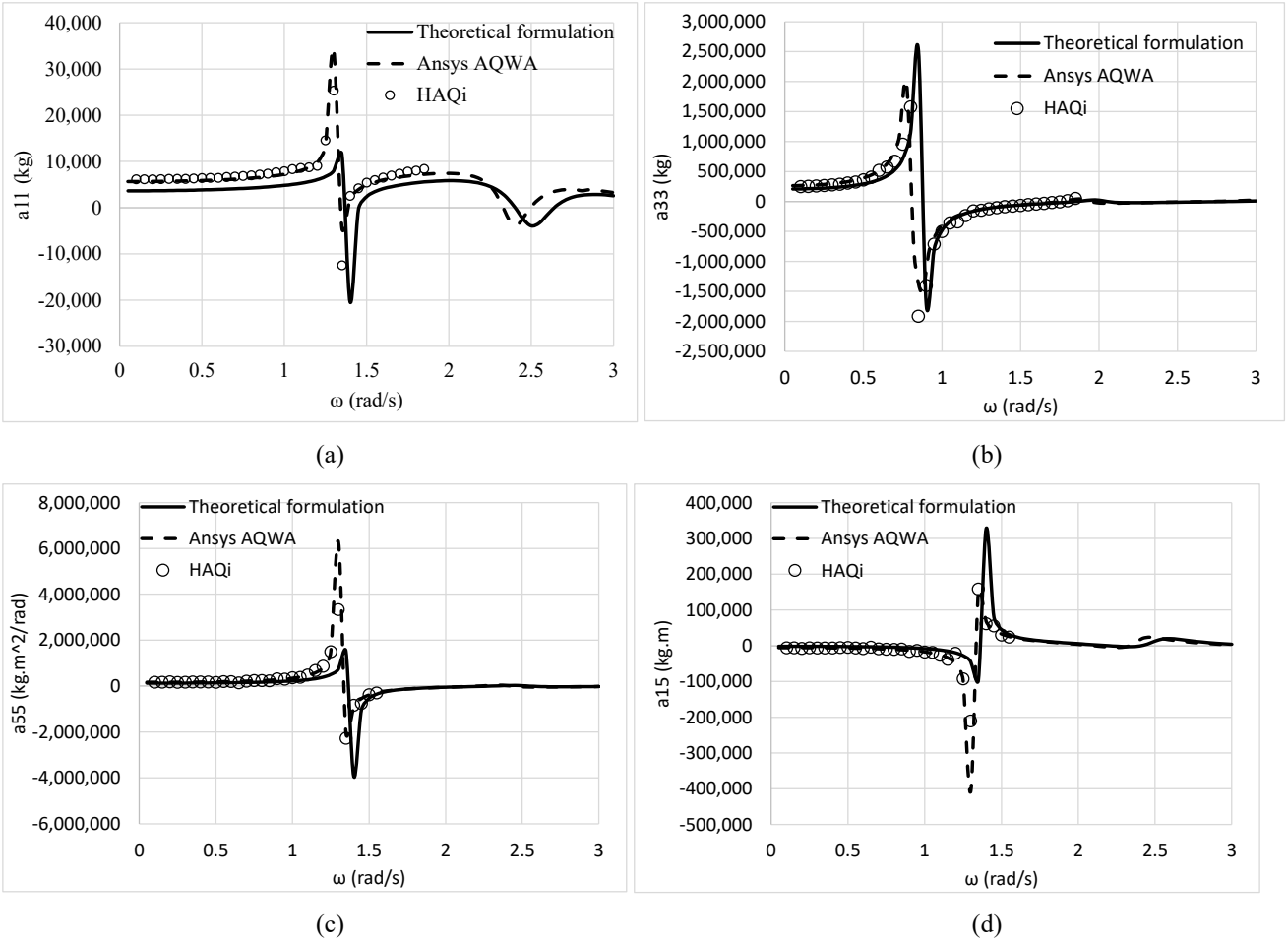

Figure 6: Hydrodynamic mass of the submerged body: (a) at the surge direction due to its forced oscillation in surge; (b) at the heave direction due to its forced oscillation in heave; (c) at the pitch direction due to its forced rotation in pitch; (d) at the surge direction due to its forced rotation in pitch

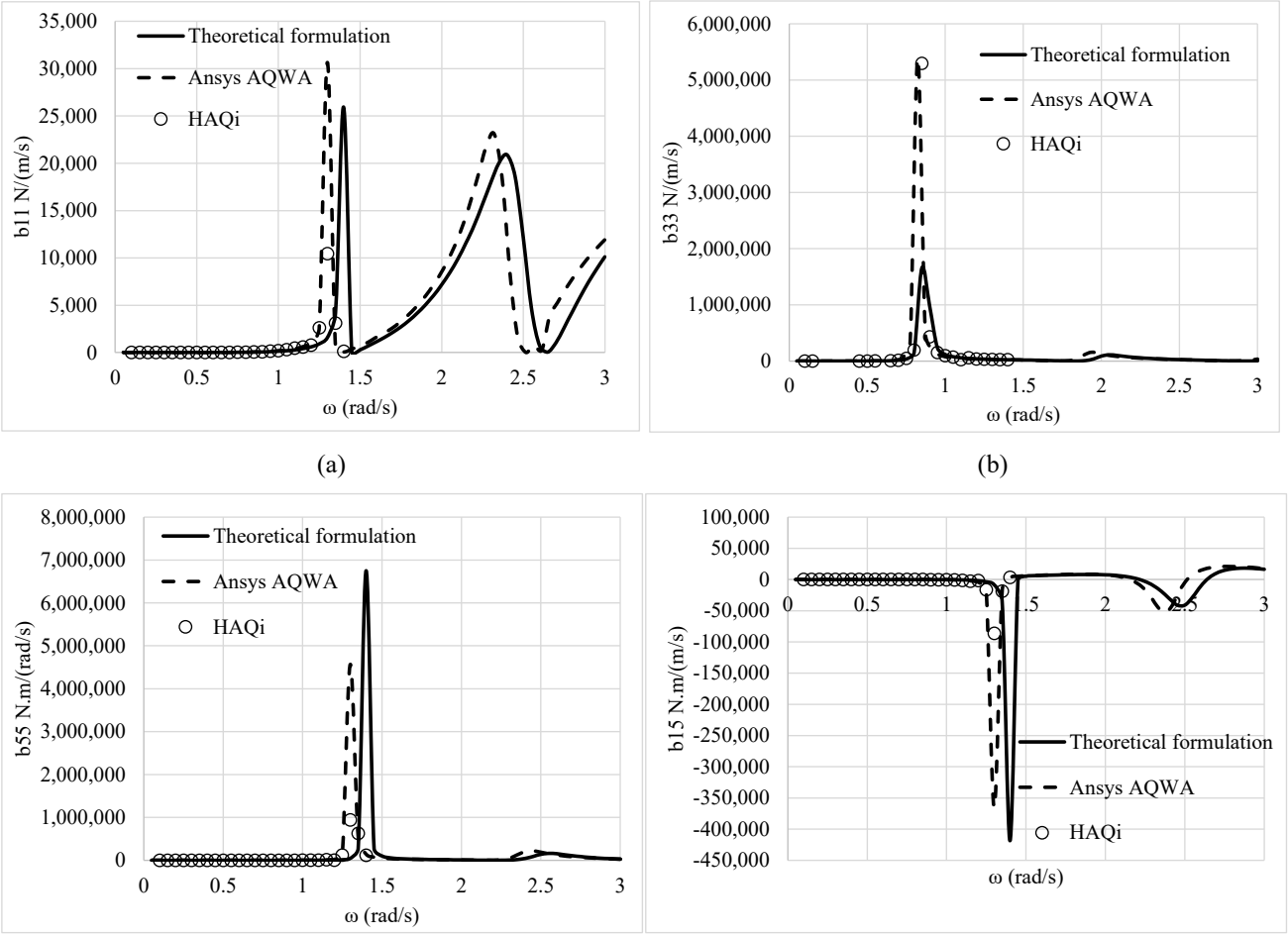

Figure 7: Damping coefficient of the submerged body: (a) at the surge direction due to its forced oscillation in surge; (b) at the heave direction due to its forced oscillation in heave; (c) at the pitch direction due to its forced rotation in pitch; (d) at the surge direction due to its forced rotation in pitch

Figure 7 illustrates the comparison of the damping coefficients $B_{11}, B_{33}, B_{55}, B_{15}$ among the three considered formulations. It is evident that B_{11}, B_{33} follow, in general, the variation pattern of the surge and heave exciting forces, characterized by peaks occurring in the neighborhood of $\omega = 1.3$rad/s and $\omega = 0.85$rad/s, respectively. It is worthwhile to note that the damping coefficients express positive values in the examined wave frequency range. Concerning the comparison between theoretical and numerical methods, it can be concluded that both numerical methods achieve comparable outcomes, whereas the theoretical analysis predicts the resonant locations at slightly higher values of wave frequencies. Nevertheless, these discrepancies are limited only near the resonant frequencies, whilst the theoretical formulation can describe accurately the hydrodynamic characteristics in the remain wave frequencies.

In Figure 8 the horizontal and vertical motions, as well as the horizontal rotations of the submerged vehicle are plotted. It can be seen that the values of x_1 decrease as the wave frequencies increase. On the other hand, x_3 begins its variation from a baseline value of one (at $\omega = 0.05$rad/s), and it increases up to $\omega = 1.7$ rad/s, where a local maximum of x_3 is attained. A smooth decrease follows leading to a local minimum of x_3 at $\omega = 1.8$ rad/s. Regarding x_5 a sharp increase is depicted in the neighborhood of $\omega = 2$ rad/s, which is followed by a prompt decrease at $\omega = 2.2$ rad/s. Furthermore, it should be noted that both the numerical models and the theoretical formulation attain similar results for the body's motions and rotations.

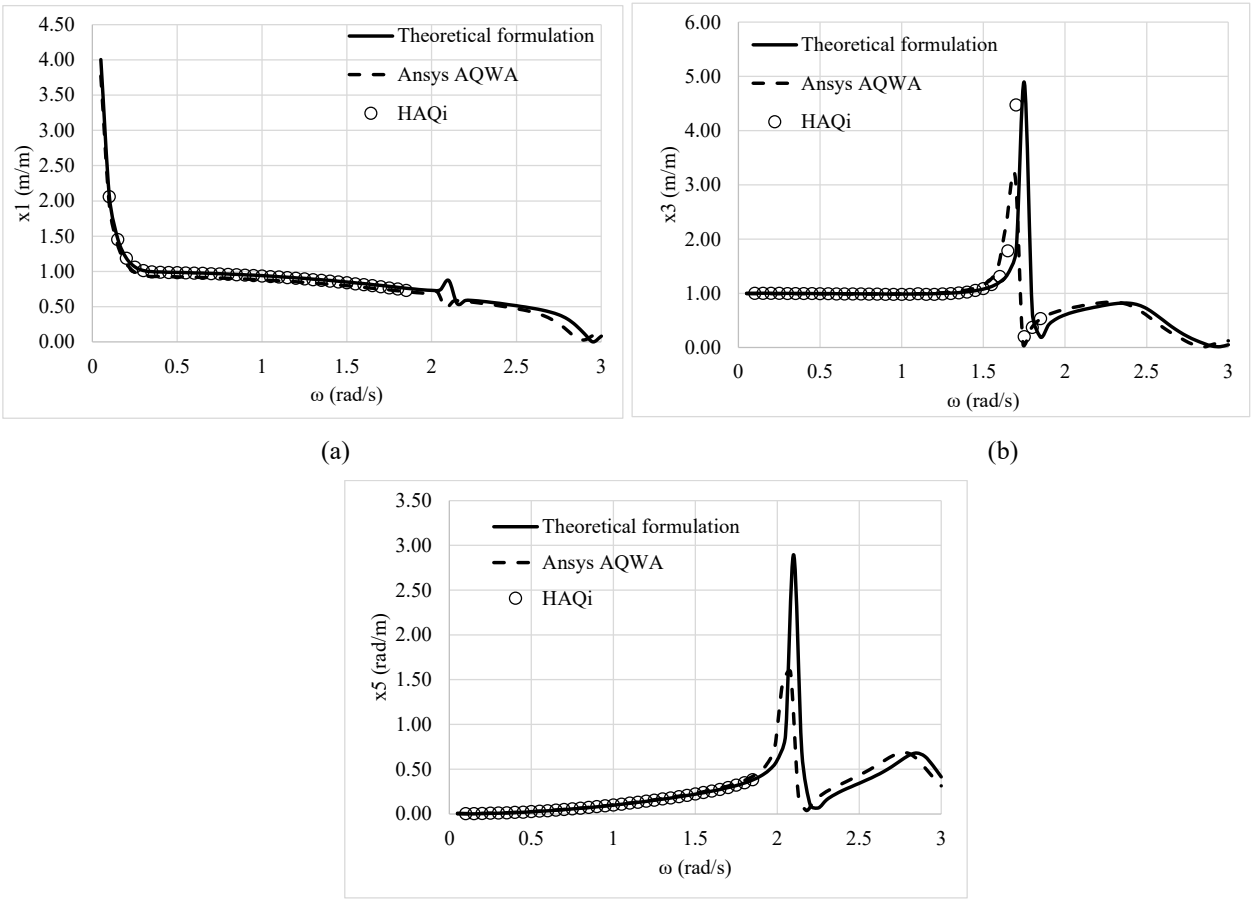

Figure 8: Motions and rotations of the submerged body: (a) horizontal motion $x_1/(H/2)$; (b) vertical motion $x_3/(H/2)$; (c) horizontal rotation $x_5/(kH/2)$

Subsequently, several submergences below free water surface are examined. Specifically, the submerged vehicle is assumed to be floating at $1h, 2h, 3h, 4h,$ below the free water surface, whereas the geometrical characteristics of the body and the water depth are remained constant. Here the outcomes are derived by the theoretical formulation, whereas the AQWA software is applied for comparative purposes for a submergence of $0h$, i.e., there exists no gap between the body's upper surface and the free water surface.

Figure 9 depicts the exciting forces and moments on the body for the various considered submergences. It can be seen that the oscillatory behavior of F_x, F_z, M_y for the $0.116h$ case is not present for higher submergences and for the scenario where the body is floating at the free surface. Furthermore, it is depicted that the exciting forces and moments decrease as the submergence increases.

Figure 10 displays the hydrodynamic coefficients of the submerged body for different levels of submergence considered. The figure illustrates that the closer to the free surface the submerged body is, the stronger the frequency dependence of the hydrodynamic parameters is. The latter is described by the decrease of sharp peaks at certain frequency ranges as the submergences increase. This also holds true for the body floating on the free surface in which no sharp peaks are presented. Therefore, it can be concluded that the hydrodynamic characteristics of the submerged cylinder undergo considerable influence by the position which is closest to the free surface. Based on McIver and Evans (1984) this can be attributed to near-standing waves which are occurred at certain wave frequencies above the submerged body at small submergence distances compared to the body's diameter.

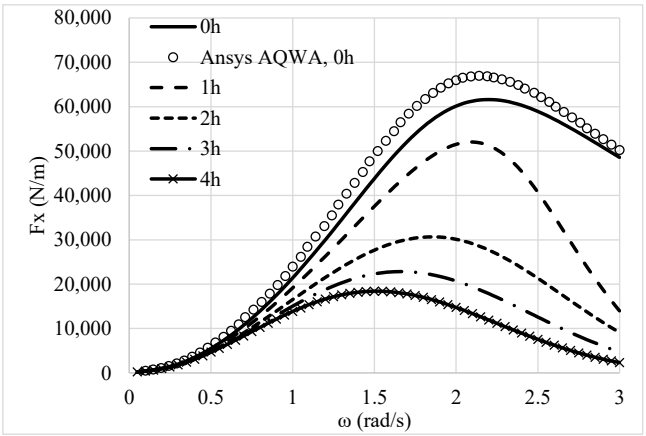

(a)

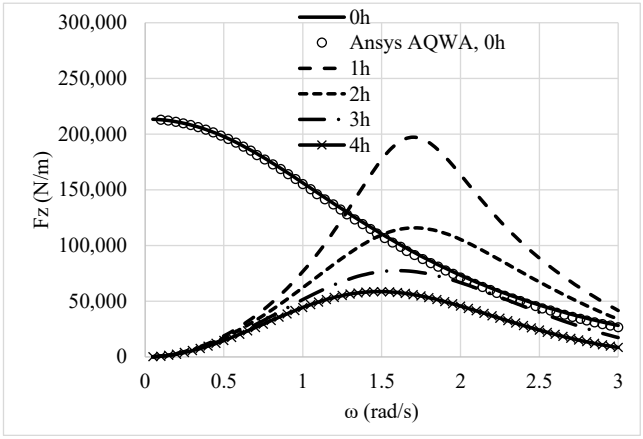

(b)

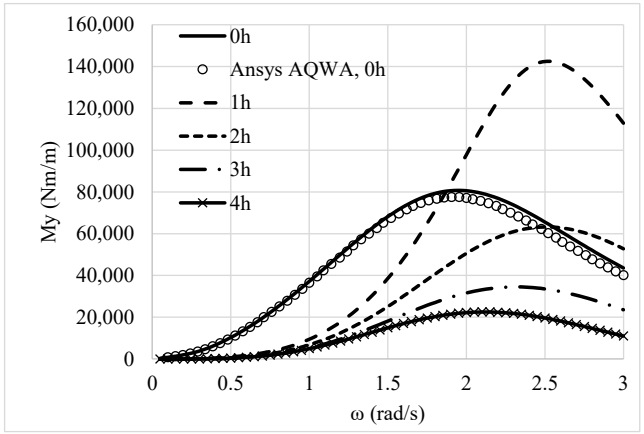

(c)

Figure 9: RAO of the exciting forces and moments on the submerged body for various submergences: (a) horizontal forces; (b) vertical forces; (c) horizontal moments

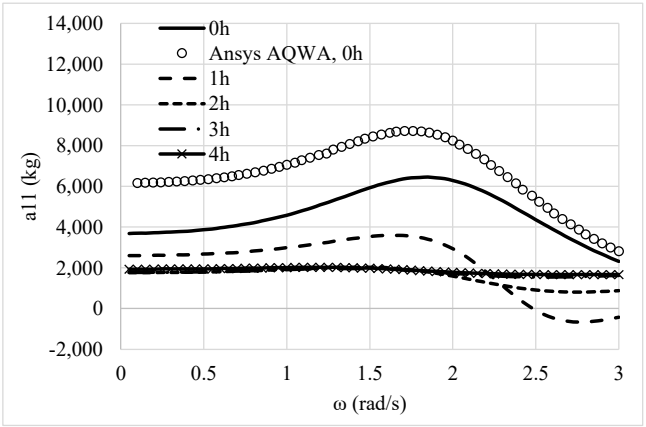

(a)

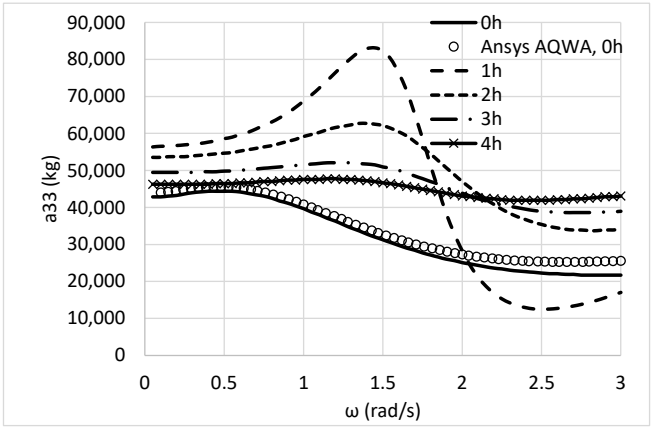

(b)

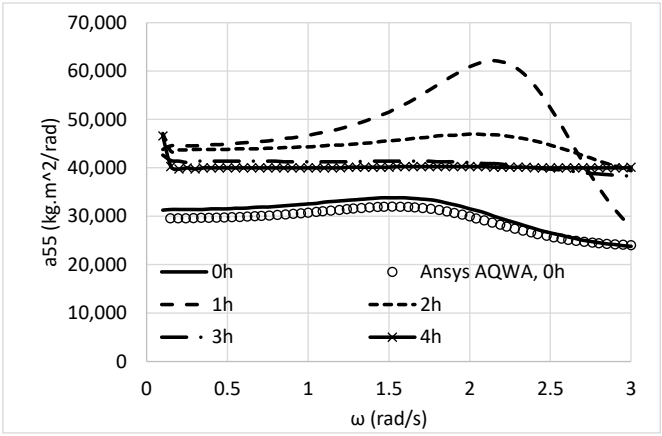

(c)

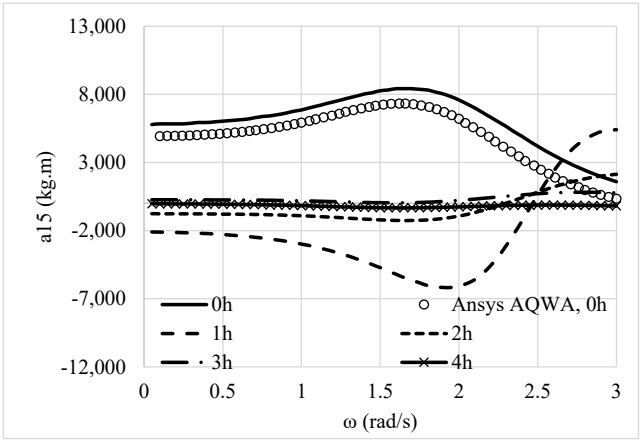

(d)

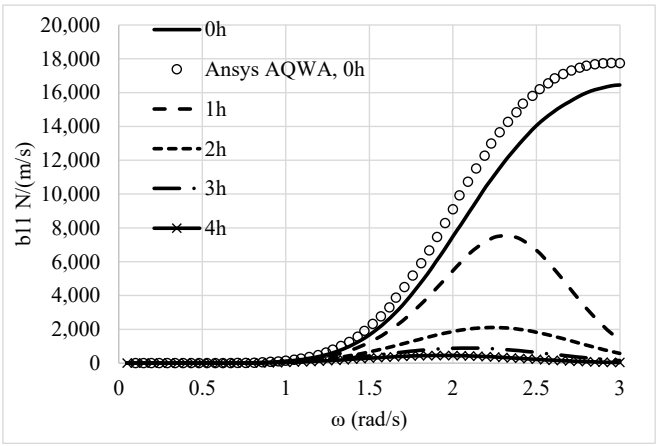

(e)

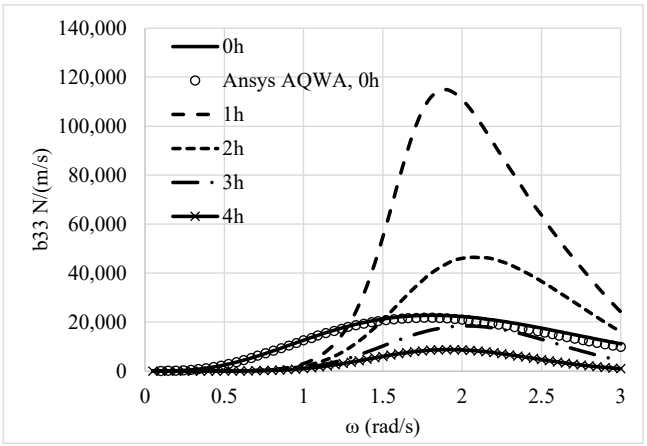

(f)

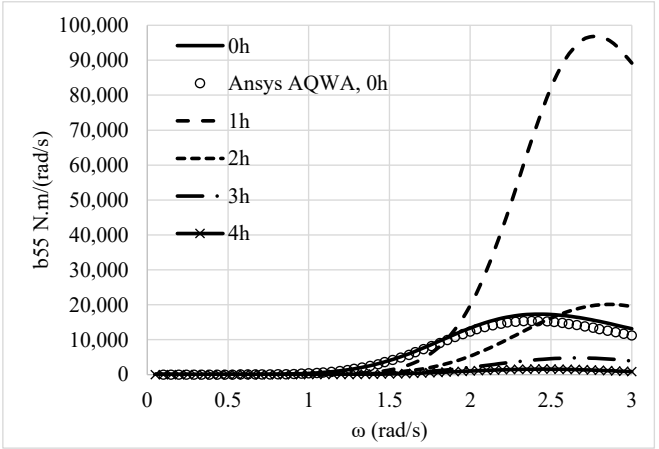

(g)

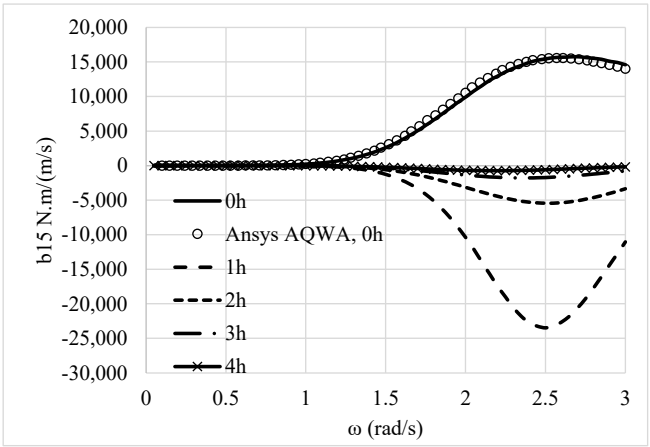

(h)

Figure 10: Hydrodynamic coefficients of the submerged body: (a) added mass at the surge direction due to its forced oscillation in surge; (b) added mass at the heave direction due to its forced oscillation in heave; (c) added mass at the pitch direction due to its forced rotation in pitch; (d) added mass at the pitch direction due to its forced oscillation in surge; (e) damping coefficient at the surge direction due to its forced oscillation in surge; (f) damping coefficient at the heave direction due to its forced oscillation in heave; (g) damping coefficient at the pitch direction due to its forced rotation in pitch; (h) damping coefficient at the pitch direction due to its forced oscillation in surge

5. CONCLUSIONS

In this paper, the effect of submergence on the hydrodynamics of an unmanned cylindrical vehicle floating below the free water surface is investigated. Three different methodologies, one theoretical and two numerical, are described and compared for various submergence distances between the body and the sea surface. The main conclusions of this study are as follows:

- the hydrodynamics of the submerged cylinder are significantly affected by the submergence of the body below the free water surface. Specifically, for small distances between the body and the free water surface sharp peaks are attained on the vehicle's hydrodynamics,
- the added mass coefficients express negative values at specific wave frequencies are noted for small submergence, which are eliminated as the body-free surface distances increase. Nevertheless, the damping coefficients express positive values in the examined wave frequency range, regardless the submergence values,
- regarding the applied methodologies, the in-house numerical software HAQi attains similar outcomes with the commercial AQWA software. Furthermore, the results from the developed theoretical formulation are perfectly aligned with the variation pattern of the outcomes from the numerical methods. However, deviations do exist at wave frequencies in which the body's hydrodynamics attain peaks.
- The findings of this analysis suggest that in near-surface operations (i.e., for a submergence depth lower than the radius of the submerged body), wave motion primarily consists of a standing wave, leading to swift alterations in both added mass and damping coefficients. Therefore, when designing submerged bodies, it's crucial to carefully consider the geometric attributes in relation to the wave characteristics since unexpected forces on the hull may be introduced increasing the inertia of the body and affecting its acceleration.

This inquiry could be expanded to explore the effect of the distance between a submerged body and the seabed on the body's hydrodynamics. Furthermore, the analysis could be further developed on the effect of various submergence distances between the free water surface and a random shaped body on the latter hydrodynamics.

DATA ACCESS STATEMENT

The data that support the findings of this study are available from the corresponding author upon reasonable request.

CONTRIBUTION STATEMENT

Mavrakos, A.: Conceptualization; methodology; writing – original draft. **Konispoliatis, D.:** Software; visualization; validation; writing – original draft, **Rossides, G.:** Visualization; writing – original draft, **Mavrakos, S.:** Methodology; software; supervision; writing – review and editing.

ACKNOWLEDGEMENTS

The DTUG prototype on which this research is based, as well as parts of this research (specifically the work performed by Dr G. Rossides), were funded by CMMI Cyprus Marine and Maritime Institute. CMMI was established by the CMMI/MaRITeC-X project as a "Center of Excellence in Marine and Maritime Research, Innovation and Technology Development" and has received funding from the European Union's Horizon 2020 research and innovation program under grant agreement No. 857586 and matching funding from the Government of the Republic of Cyprus.

REFERENCES

Abramowitz, M., Stegun, I. 1970. Handbook of Mathematical Functions, Dover Publications, Inc., New York
Amiri, M.M.; Esperana, P.; Vitola, M.A.; Sphaier, S.H. (2018). How does the free surface affect the hydrodynamics of a shallowly submerged submarine? Applied Ocean Research 76, 34-50. https://doi.org/10.1016/j.apor.2018.04.008
Amiri, M.M.; Esperana, P.; Vitola, M.A.; Sphaier, S.H. (2019a). An initial evaluation of the free surface effect on the maneuverability of underwater vehicles. Ocean Engineering 196, 106851. https://doi.org/10.1016/j.oceaneng.2019.106851
Amiri, M.M.; Esperana, P.; Vitola, M.A.; Sphaier, S.H. (2019b). Investigation into the wave system of a generic submarine moving along a straight path beneath the free surface. European Journal of Mechanics – B/Fluids 76, 98-114. https://doi.org/10.1016/j.euromechflu.2019.02.006
Amiri, M.M.; Esperana, P.; Vitola, M.A.; Sphaier, S.H. (2020). Viscosity effect on an underwater vehicle-free surface

hydrodynamic interaction. Applied Ocean Research 104, 102365. https://doi.org/10.1016/j.apor.2020.102365
ANSYS AQWA Theory Manual, 2015. ANSYS Inc. Southpointe 2600 ANSYS Drive Canonsburg, PA 15317
Arentzen, E.S.; Mandel, P. (1960). Naval architectural aspects of submarine design. The Society of Naval Architects and Marine Engineers
Bardis, L.; Mavrakos, S. (1988). User's manual for the computer code HAQ. Laboratory for Floating Bodies and Mooring Systems, National Technical University of Athens
Benusiglio, A.; Chevy, F.; Raphael, E.; Clanet, C. (2015). Wave drag on a submerged sphere. Physics of Fluids 27, 07210. https://doi.org/10.1063/1.4923454
Burcher, R.; Rydill, L.J. (1995). Concepts in submarine design. Cambridge University Press. https://doi.org/10.1017/CBO9781107050211
Chepelianskii, A.; Schindler, M.; Chevy, F.; Raphael, E. (2010). Self-consistent theory of capillary–gravity-wave generation by small moving objects. Physical Review E, 81, 016306. https://doi.org/10.1103/PhysRevE.81.016306
Chung, J.S. (1977). Forces on submerged cylinders oscillating near free surface. Journal of Hydronautics, 11(3), 100-106. https://doi.org/10.2514/3.63081
Choi, J.H.; Yeo, D.J.; Rhee, K.P.; Park, J.Y. (2006). On the vertical plane dynamics modeling and depth control of a submerged body moving beneath free surface. Journal of the Society of Naval Architects of Korea 43(6), 647-655. https://doi.org/10.3744/SNAK.2006.43.6.647
Choi, J.H.; Rhee, K.P.; Ann, S.P.; Lee, S.K. (2008). Mathematical model of wave forces and moments for the depth control of a submerged body. Proceedings of the Annual Spring Meeting of the Society of Naval Architects of Korea, 1228-1235
Conway, A.S.T.; Valentinis, F.; Seil, G. (2018). Characterization of suction effects on a submarine body operating near the free surface. Proceedings of the 21st Australian Fluid Mechanics Conference, 10-13 November, Adelaide, Australia.
Fossen, T. I. (2011). Handbook of Marine Craft Hydrodynamics and Motion Control. John Wiley & Sons, Ltd. https://doi.org/https://doi.org/10.1002/9781119994138.ch2
Garrison, C.J. (1974). Hydrodynamics of large objects in the sea. Part I: Hydrodynamic analysis. Journal of Hydronautics 8, 5-12. https://doi.org/10.2514/3.62970
Garrison, C.J. (1975). Hydrodynamics of large objects in the sea. Part II: Motion of free floating bodies. Journal of Hydronautics 9, 58-63. https://doi.org/10.2514/3.63020
Hao, Y.; Shen, D.; Xiong, Z. (2004). Design of submarine near-surface depth controller. Proceedings of the 5th World Congress on Intelligent Control and Automation, 15-19 June, Hangzhou, China. https://doi.org/10.1109/WCICA.2004.1342374
Havelock, T.H. (1917). Some cases of wave motion due to a submerged obstacle. Proceedings of the Royal Society A 93, 520-532. http://doi.org/10.1098/rspa.1917.0036
Havelock, T.H. (1931). The wave resistance of a spheroid. Proceedings of the Royal Society A 131, 275-285. http://doi.org/10.1098/rspa.1931.0052
Jagadeesh, P.; Murali, K.; Idichandy, V.G. (2009). Experimental investigation of hydrodynamic force coefficients over AUV hull form. Ocean Engineering 36, 113-118. https://doi.org/10.1016/j.oceaneng.2008.11.008
Javaid, M. Y., Ovinis, M., Nagarajan, T., & Hashim, F. B. M. (2014). Underwater Gliders: A Review. MATEC Web of Conferences, 13, 2020. https://doi.org/10.1051/matecconf/20141302020
Lambert, W.; Brizzolara, S. (2020). On the effect of non-linear boundary conditions on the wave disturbance and hydrodynamic forces of underwater vehicles travelling near the free-surface. Proceedings of the 39th International Conference on Ocean, Offshore and Arctic Engineering, The American Society of Mechanical Engineers, 3-7 August, Fort Lauderdale, FL, USA
Ling, X.; Leong, Z.Q.; Duffy, J. (2023). Effects of pitch angle on a near free surface underwater vehicle. Ocean Engineering 286, 115611. https://doi.org/10.1016/j.oceaneng.2023.115611
Kokkinowrachos, K.; Mavrakos, S.; Asorakos, S. (1986). Behavior of vertical bodies of revolution in waves. Ocean Engineering 13, 505 – 538.
Mansoorzadeh, S.; Javanmard, E. (2014). An investigation of free surface effects on drag and lift coefficients of an autonomous underwater vehicle (AUV) using computational and experimental fluid dynamics methods. Journal of Fluids and Structures 51, 161-171. https://doi.org/10.1016/j.jfluidstructs.2014.09.001
Mavrakos, S.A.; Bardis, L. (1984). Hydrodynamic characteristics of large offshore units. Proceedings of the 3rd International Congress on Marine Technology (IMAM), 28 May – 1 June, Athens, Greece
Mavrakos, S.A. (1985). Wave loads on a stationary floating bottomless cylindrical body with finite wall thickness. Applied Ocean Research 7(4), 213 – 224. https://doi.org/10.1016/0141-1187(85)90028-8
Mavrakos, S.A. (1988). Hydrodynamic coefficients for a thick-walled bottomless cylindrical body floating in water of finite depth. Ocean Engineering, 15(3), 213 – 229. https://doi.org/10.1016/0029-8018(88)90040-6
Mavrakos, S.A. (1993). Hydrodynamic characteristics for groups of interacting axisymmetric bodies submerged near the sea surface or the sea bed. Proceedings of the 3rd International Offshore and Polar Engineering Conference, 6-11 June, Singapore
Mavrakos, S.A. (1995). Users manual for the software HAMVAB. School of Naval Architecture and Marine Engineering, Laboratory for Floating Structures and Mooring Systems, Athens, Greece
Mavrakos, S.A. (2004). Hydrodynamic coefficients in heave of two concentric surface-piercing truncated circular cylinders. Applied Ocean Research 26(3–4), 84–97. https://doi.org/10.1016/j.apor.2005.03.002

McIver, P., Evans, D.V. (1984). The occurrence of negative added mass in free-surface problems involving submerged oscillating bodies. Journal of Engineering Mathematics 18, 7–22
Michell, J.H. (1898). The wave-resistance of a ship. The London, Edinburgh, and Dublin Philosophical Magazine and Journal of Science, 45:272, 106-123, http://dx.doi.org/10.1080/14786449808621111
Nakamura, M., Hyodo, T., & Koterayama, W. (2007). "LUNA" Testbed Vehicle For Virtual Mooring. All Days.
Nakamura, M., Koterayama, W., Inada, M., Marubayashi, K., Hyodo, T., Yoshimura, H., & Morii, Y. (2008). Disk Type Underwater Glider For Virtual Mooring And Field Experiment. All Days.
Nematollahi, A.; Dadvand, A.; Dawoodian, M. (2015). An axisymmetric underwater vehicle-free surface interaction: a numerical study. Ocean Engineering 96, 205-214. http://dx.doi.org/10.1016/j.oceaneng.2014.12.028
Newman, J.N.; Sortland, B.; Vinje, T. (1984). Added mass and damping of rectangular bodies close to the free surface. Journal of Ship Research 28(4), 219-225. https://doi.org/10.5957/jsr.1984.28.4.219
Ogilvie, T.F. (1963). First- and second- order forces on a cylinder submerged under a free surface. Journal of Fluid Mechanics, 16(3), 451-472. https://doi.org/10.1017/S0022112063000896
Park, J.Y.; Kim, N.; Yoon, H.K.; Cho, H. (2016). Adaptive depth controller design for a submerged body moving near free surface. Applied Ocean Research 58, 83-94. http://dx.doi.org/10.1016/j.apor.2016.04.001
Rezazadegan, F.; Shojaei, K.; Sheikholeslam, F.; Chatraei, A. (2015). A novel approach to 6-DOF adaptive trajectory tracking control of an AUV in the presence of parameter uncertainties. Ocean Engineering 107, 246-258. http://dx.doi.org/10.1016/j.oceaneng.2015.07.040
Shao, Z.; Chen, Y.; Fang, D.; Feng, S. (2012). Fuzzy depth control of small cylindrical object navigating near free-surface. Applied Mechanics and Materials 128(129), 886-889. https://doi.org/10.4028/www.scientific.net/AMM.128-129.886
Sudharsun, G.; Ali, A.; Mitra, A.; Jaiswal, A.; Naresh, P.; Warrior, H.V. (2022). Free surface features of submarines moving underwater: study of Bernoulli Hump. Ocean Engineering 249, 110792. https://doi.org/10.1016/j.oceaneng.2022.110792
Wehausen, J.V.; Laitone, E.V. (1960). Surface Waves. In Encyclopedia of Physics; Springer: Berlin/Heidelberg, Germany, Volume 9
Yu, P., Wang, T., Zhou, H., & Shen, C. (2017). Dynamic modeling and three-dimensional motion simulation of a disk type underwater glider. International Journal of Naval Architecture and Ocean Engineering, 10. https://doi.org/10.1016/j.ijnaoe.2017.08.002
Zemlyak, V.; Pogorelova, A.; Kozin, V. (2022). Motion of a submerged body in a near-surface water environment. International Journal of Naval Architecture and Ocean Engineering 14, 100433. https://doi.org/10.1016/j.ijnaoe.2021.100433
Zemlyak, V.; Pogorelova, A.; Kozin, V. (2023). Motion of a submerged body under a free surface and an ice cover in finite water depth conditions. Ocean Engineering 288, 116161. https://doi.org/10.1016/j.oceaneng.2023.116161
Zhou, H., Yu, P., Jin, X., & Wang, T. (2020). Analysis of the In Situ Steering Motion Characteristics and Sensitivity of Disc-Type Underwater Gliders. Journal of Marine Science and Engineering, 8, 663. https://doi.org/10.3390/jmse8090663